

# Stacking-sliding and irradiation-direction invariant Floquet altermagnets in A-type antiferromagnetic bilayers

Zhe Li,<sup>1,\*</sup> Lijuan Li,<sup>2</sup> Mengxue Guan,<sup>2</sup> and Sheng Meng<sup>1,3,4</sup>

<sup>1</sup>*Beijing National Laboratory for Condensed Matter Physics, and Institute of Physics, Chinese Academy of Sciences, Beijing 100190, China*

<sup>2</sup>*Centre for Quantum Physics, Key Laboratory of Advanced Optoelectronic Quantum Architecture and Measurement (Ministry of Education), School of Physics, Beijing Institute of Technology, Beijing 100081, China*

<sup>3</sup>*University of Chinese Academy of Sciences, Beijing 100049, China*

<sup>4</sup>*Songshan Lake Materials Laboratory, Dongguan, Guangdong 523808, China*

(Dated: December 9, 2025)

Arranging the stacking orders of A-type antiferromagnetic (A-AFM) bilayers offers an accessible pathway to two-dimensional altermagnets, but requires strict symmetry conditions such as layer groups, sliding positions, and twisting angles. Here, we find that circularly polarized light (CPL) irradiation breaks time-reversal symmetry, enabling the development of altermagnets beyond these constraints. Based on symmetrical analysis, our revealments indicate that A-AFM bilayer building-blocks with inversion symmetry exhibit altermagnetism robust to stacking sliding and variations of illumination directions. These bilayers can be constructed from arbitrary ferromagnetic monolayers and guided by the  $d$ -electron counting rule. Adopting bilayer  $\text{MnBi}_2\text{Te}_4$  as a template, out-of-plane illumination with CPL reveals an  $f$ -wave altermagnetic feature at sliding positions  $\{E| (0, 0)\}$ ,  $\{E| (\frac{1}{3}, \frac{2}{3})\}$  and  $\{E| (\frac{2}{3}, \frac{1}{3})\}$ , while a  $p$ -wave feature is predicted at other sliding positions. Our unveilings popularize the applicability of altermagnets in A-AFM bilayers with inversion symmetry, igniting a new wave of research in this field.

Recently, the simplification and popularization of material design for altermagnets have emerged as one of the most dynamic fields of research [1–10]. Altermagnets, characterized by the absence of net magnetization yet exhibiting symmetrical spin splitting in certain regions of the Brillouin zone (BZ), represent a remarkable form of unconventional magnetism [1–10]. The spin-space operators inherent in these materials cause spin degeneracy at specific points, lines, or planes, creating boundaries that separate regions of opposite spin splitting. The diverse geometries of these boundaries result in spin-dependent Fermi surfaces with planar or bulk  $d$ -wave,  $g$ -wave, or  $i$ -wave symmetries [1–5]. Thus far, a variety of materials have been theoretically predicted or experimentally confirmed as altermagnets, including  $\text{MnTe}$  [11–13],  $\text{CrSb}$  [14–16],  $\text{RuO}_2$  [17–20],  $\text{KV}_2\text{Se}_2\text{O}$  [21, 22],  $\text{Rb}_{1-\delta}\text{V}_2\text{Te}_2\text{O}$  [23],  $\text{Nb}(\text{V})_2\text{SeTeO}$  [5, 24–26],  $\text{NiZrI}_6$  [27–29], among others [30–37]. Notably, altermagnets exhibit unique behaviors in a range of novel physical phenomena, such as the significant anomalous Hall effect [18, 34, 35, 38, 39], the anomalous Nernst effect [36, 40], crystal thermal transport [20], piezomagnetism [29, 41], piezoelectricity [42], spin-splitter torque [19, 43], the magneto-optical effect [37, 44], chiral magnons [17], the type-II quantum spin Hall effect [25], and beyond [19, 43].

Among the scenarios discussed, a straightforward approach to constructing altermagnets involves the precise arrangement of A-type antiferromagnetic (A-AFM) bilayers with specific stacking orders, as guided by general

stacking theory [6, 27, 28, 45]. However, this method imposes strict requirements on the bilayers. Firstly, only 17 out of 80 layer groups possess the inherent potential for altermagnetism, with only the operators  $C_{2\alpha}$  or  $S_{4z}$  supporting this phenomenon [28]. Secondly, the stacking theory for altermagnets is highly dependent on particular stacking orders, such as sliding or twisted angles [6, 27, 28, 45, 46], which necessitate relatively stringent experimental conditions. Moreover, the presence of inversion symmetry ( $[C_2||P]$ ) and mirror symmetry with respect to the  $x$ - $y$  plane ( $[C_2||M_z]$ ) acts antagonistically to the formation of altermagnets [27, 28, 47], with the former being prevalent in most conventional materials.

Noteworthy, Floquet engineering using circularly or elliptically polarized light (CPL or EPL) opens up new pathways for odd-parity altermagnets [47–51]. In contrast to the previously discussed altermagnets that possess time-reversal symmetry ( $[C_2||T]$ ), which enforces an even-parity relationship  $\varepsilon(\mathbf{k}, s) = \varepsilon(-\mathbf{k}, s)$ , the excitation of CPL or EPL breaks this symmetry [47–51]. This not only allows for the emergence of odd-parity waves but also broadens the range of altermagnets that were previously constrained by the presence of inversion symmetry  $[C_2||P]$  or mirror symmetry with respect to the  $x$ - $y$  plane  $[C_2||M_z]$ . This insight suggests that altermagnetism is likely to be realized in the majority of conventional A-AFM bilayer systems.

In this work, through a detailed symmetrical analysis of the spin-space group, we prove that under the Floquet engineering of CPL or EPL, all A-AFM bilayers with inversion symmetry exhibit odd-parity altermagnetism, independent of stacking sliding or irradiation angles. By duplicating any ferromagnetic (FM) monolayer using a

\* lizhe21@iphy.ac.cn

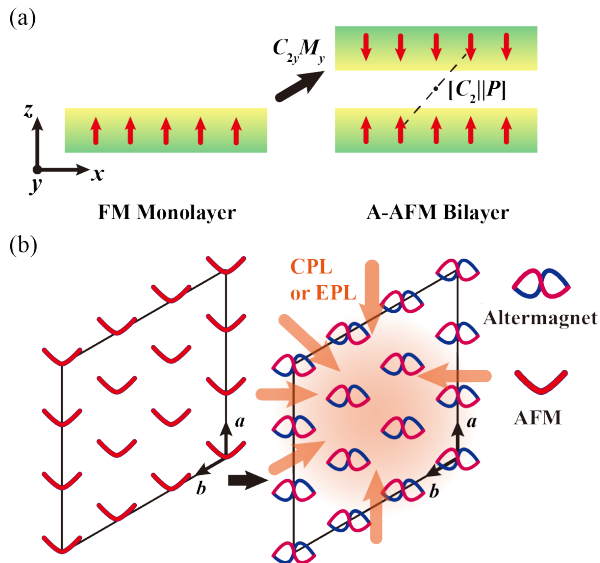


FIG. 1. **Schematic of building Floquet altermagnets.** (a) Constructing strategy of an A-AFM bilayer with  $[C_2||P]$  from a FM monolayer. The yellow and green regions represent the top and bottom parts of the FM monolayer, respectively, while the red arrows indicate the magnetic moments. (b) The sliding-invariant AFM state is Floquet-engineered into the sliding-invariant altermagnetic state regardless of illumination directions.

combined operation of  $C_{2y}M_y$  relative to a point slightly above the first layer, the aforementioned A-AFM bilayer can be constructed according to the  $d$ -electron counting rule [52–54]. The only exception is  $[C_2||M_z]$ , which inadvertently suppresses altermagnetism solely under  $z$ -axis irradiation. Among various candidate A-AFM bilayers possessing  $[C_2||P]$ , we employ bilayer  $\text{MnBi}_2\text{Te}_4$  (BL-MBT) as a benchmark. Forward-stacking BL-MBT displays  $f$ -wave altermagnetism when irradiated with CPL along the  $z$ -axis. It transitions to  $p$ -wave altermagnetism with stacking sliding or varying incident angles, except at specific sliding positions  $\{E|(\frac{1}{3}, \frac{2}{3})\}$  and  $\{E|(\frac{2}{3}, \frac{1}{3})\}$ . Our discovery and proposal highlight the widespread potential of altermagnetism in A-AFM bilayers with inversion symmetry, offering a most prevalent and unsophisticated designing method for altermagnets to date.

Here, we focus on a nonrelativistic perspective that excludes spin-orbit coupling effects. Consequently, the spin-space group  $[R_s||R_l]$ , along with time-reversal symmetry  $[R_s||T]$ , is appropriately suited for a symmetrical description, where  $R_s$  and  $R_l$  represent the spin and space groups, respectively. For stacking operations, we adopt the notation  $\{G|\tau\}$ , where  $G$  denotes the point group operations and  $\tau$  represents the sliding operations.

From the perspective of stacking sliding, the condition  $E \cap P = 0$  ensures that the stacking sliding operation  $\{E|\tau\}$  is completely decoupled from  $P$ , thereby preserving the invariance of  $[C_2||P]$ . Furthermore, for CPL and EPL, regardless of incident angles, a time reversal operation yields:  $TA(t) \rightarrow -A(-t)$ , while a spatial reversal

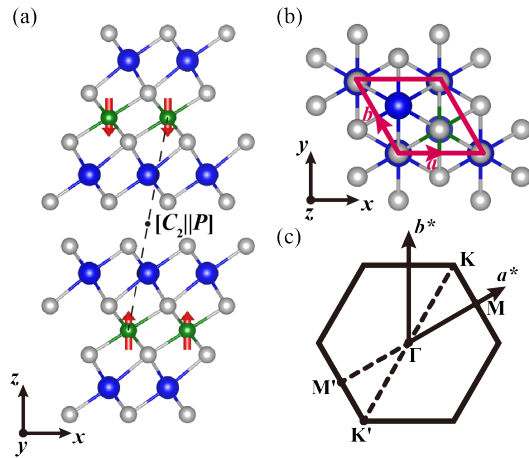


FIG. 2. **Illustrations of BL-MBT under normal stacking with (a) side view, (b) top view and (c) first BZ zone.** The green, blue, and gray spheres represent Mn, Bi, and Te atoms, respectively. The red arrows in panel (a) indicate the direction of the magnetic moments. In panel (b), the red rhombus denotes the stacking-sliding zone.

operation gives:  $PA(t) \rightarrow -A(t)$ . Although the potential vector temporarily reverses direction, it's important to note that Floquet engineering is an accumulated effect over several cycles [55–58]. Therefore, the chirality of the light prevails over its transient value, which remains invariant (changes sign) after the operation of  $P$  ( $T$ ). Consequently,  $[C_2||P]$  remains intact, while  $[C_2||T]$  is broken, regardless of stacking sliding or light incident directions. This conclusion is also in accordance with the Floquet-Bloch theory [59–61].

Remarkably, A-AFM bilayers characterized by  $[C_2||P]$  can be constructed from any arbitrary FM monolayer, provided that the interlayer coupling is AFM driven by the  $d$ -electron counting rule [52–54]. Figure 1(a) illustrates a straightforward method towards this. First, identify an operation center located just above the FM monolayer. Next, duplicate this monolayer after applying a  $C_{2y}$  rotation, which transforms the coordinates  $(x, y, z)$  to  $(-x, y, -z)$ , followed by a mirror operation with respect to the  $x$ - $z$  plane (denoted as  $M_y$ ), resulting in the final coordinates of  $(-x, -y, -z)$ . This sequence of operations effectively achieves inversion symmetry, as depicted in the right panel of Fig. 1(a). Thus, we propose a straightforward and universal method for creating a Floquet altermagnet from a FM monolayer, independent of stacking-sliding and CPL incident angle constraints, provided the interlayer coupling is AFM. Figure 1(b) conspicuously illustrates this innovation. Candidate materials include bilayer  $\text{MnBr}_2$ ,  $\text{CoBr}_2$ ,  $\text{NiBr}_2$ ,  $\text{FeBr}_2$ ,  $\text{MnBi}_2\text{Te}_4$  and  $\text{LiFeSe}$ , among others [52, 53, 62, 63].

Next, let's focus on BL-MBT as a representative template. As a prominent magnetic topological insulator, MBT exhibits FM coupling in its monolayer form and interlayer AFM coupling in bilayer configurations, characterized by the atomic stacking sequence "ABCABC..."

TABLE I. Space groups of forward stacking BL-MBT resulting from various stacking sliding operations.

Space Groups	Notations	Representative stacking operators
No. 164	$P\bar{3}m1$	$\{E (0,0)\}, \{E (\frac{1}{3}, \frac{2}{3})\}, \{E (\frac{2}{3}, \frac{1}{3})\}$
No. 12	$C2/m$	$\{E (\frac{1}{6}, \frac{5}{6})\}, \{E (\frac{1}{2}, 0)\}, \{E (\frac{1}{2}, \frac{1}{2})\}, \{E (0, \frac{1}{2})\}, \{E (\frac{5}{6}, \frac{1}{6})\}, \{E (\frac{1}{6}, \frac{1}{3})\}, \{E (\frac{1}{3}, \frac{1}{6})\},$ etc.
No. 2	$P\bar{1}$	$\{E (\frac{1}{6}, 0)\}, \{E (0, \frac{1}{6})\}, \{E (\frac{1}{3}, 0)\}, \{E (0, \frac{1}{3})\}, \{E (\frac{1}{2}, \frac{5}{6})\}, \{E (\frac{1}{2}, \frac{1}{6})\}, \{E (\frac{1}{3}, \frac{1}{3})\},$ etc.

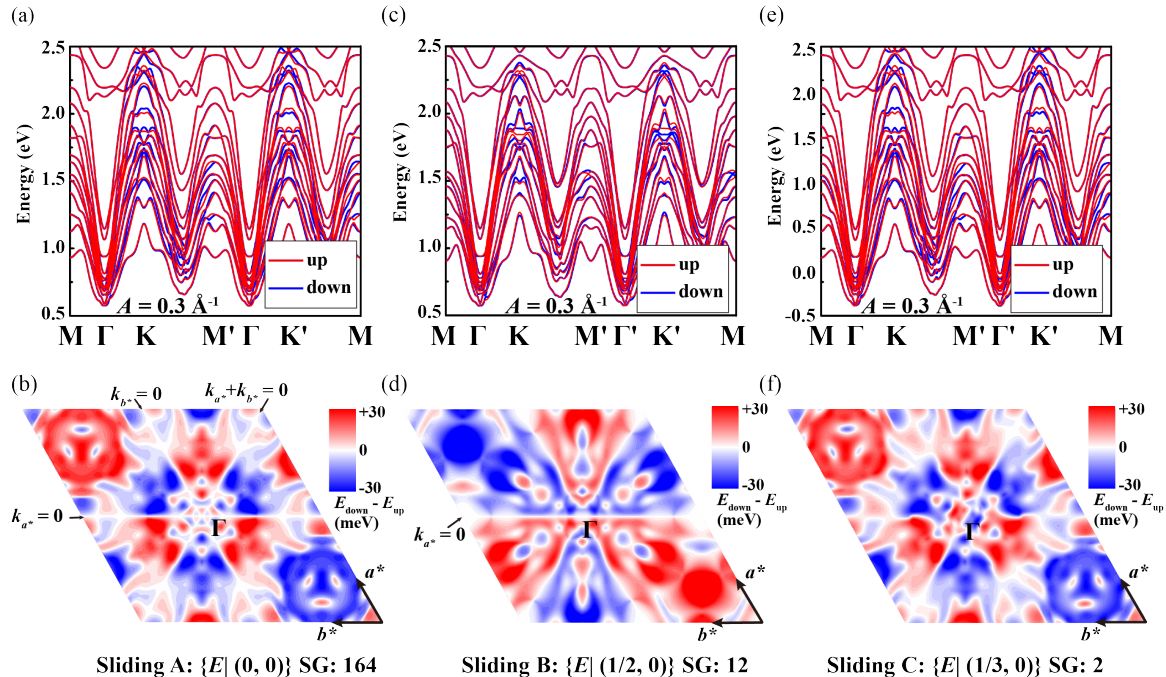


FIG. 3. BL-MBT: band structures along high-symmetry lines and spin-splitting distributions in three types of stacking sliding positions, with the light frequency and incident direction set to  $\hbar\omega = 9.0$  eV and along  $z$ -axis respectively. Panel (a) exhibits the spin-resolved band structures along the high-symmetry lines  $M$ - $\Gamma$ - $K$ - $M'$ - $\Gamma$ - $K'$ - $M$  under the light intensity of  $0.3 \text{ \AA}^{-1}$ . The red and blue curves represent spin-up and spin-down states, respectively. Panel (b) illustrates the contour distributions of spin-splitting energies across the entire BZ, with the color gradient ranging from white to red (positive values) and blue (negative values), reflecting the relationship:  $E_{\text{down}} - E_{\text{up}}$ . The occupancy number of the Wannier bands is 83. Panels (a) and (b) correspond to the normal stacking order ( $\{E|(0,0)\}$ ). Panels (c) and (d), (e) and (f) are analogous to (a) and (b), but for the stacking sliding positions  $\{E|(\frac{1}{2}, 0)\}$  and  $\{E|(\frac{1}{3}, 0)\}$  respectively.

[53, 54, 62, 64–74]. BL-MBT crystallizes in a trigonal lattice and belongs to space group No. 164 ( $P\bar{3}m1$ ), guaranteeing the presence of  $P$  throughout the system. Subsequently, the two atomic layers of Mn with opposite spins are connected by the symmetries  $[C_2||P]$  and  $[C_2||T]$ , resulting in spin degeneracy across the entire BZ.

Figure 2(a) presents a side view of BL-MBT in its normal configuration, referred as “forward stacking”. The sliding operations are depicted in Fig. 2(b), illustrating the top view of BL-MBT with forward stacking. Although the stacking-sliding maintains the symmetry  $[C_2||P]$ , it reduces the overall symmetry of the system. Table I presents three types of space groups resulting from various sliding operations in forward stacking, categorized as No. 164 ( $P\bar{3}m1$ ), No. 12 ( $C2/m$ ) and No. 2 ( $P\bar{1}$ ). Only the first group, associated with stacking orders  $\{E|(0,0)\}$ ,  $\{E|(\frac{1}{3}, \frac{2}{3})\}$  and  $\{E|(\frac{2}{3}, \frac{1}{3})\}$ , retains

$C_{3z}$ -rotational symmetry. The lattice vectors and the shape of the first BZ are illustrated in Fig. S1, encompassing all the space groups relevant to this work.

For simplicity, we consider CPL incident along the  $z$ -axis. In the context of space group No. 164, which corresponds to normal stacking (denoted as sliding A), the remaining operators connecting the two atomic layers of Mn include  $[C_2||P]$ ,  $[C_2||PC_{3z}^1]$ ,  $[C_2||PC_{3z}^2]$ ,  $[E||C_{2a}T]$ ,  $[E||C_{2b}T]$  and  $[E||C_{2ab}T]$ . These spin-space group operators lead to a threefold distribution of spin-degenerate lines at  $k_{a^*} = k_{b^*} = k_{a^*} + k_{b^*} = 0$ . Figure 3(a) displays spin-resolved band structures along the high-symmetry lines of  $M$ - $\Gamma$ - $K$ - $M'$ - $\Gamma$ - $K'$ - $M$  [as illustrated in the first BZ in Fig. 2(d)] under the light intensity of  $0.3 \text{ \AA}^{-1}$ . A high-frequency regime is employed ( $\hbar\omega = 9.0$  eV) to prevent the mixing of zero-order bands with their replicas.

The condition with the light intensity of  $0.0 \text{ \AA}^{-1}$  (see

Fig. S2) performs no observable Floquet-engineering effect, as the two spins remain degenerate throughout, thereby maintaining an AFM state. In contrast, the light intensity of  $0.3 \text{ \AA}^{-1}$  induces a significant Floquet-engineering effect, characterized by the states of the two spins splitting in opposite directions along the positive line  $M\text{-}\Gamma\text{-}K\text{-}M'$  and the negative line  $M'\text{-}\Gamma\text{-}K'\text{-}M$ . This behavior provides strong evidence for odd-parity altermagnetism, which is further corroborated by the distribution of spin-splitting energies throughout the entire BZ [see Fig. 3(b)]. Three white spin-degenerate lines, arranged at  $60^\circ$  angles to each other, delineate the regions of opposite spin splitting, consistent with the remaining spin-space group operators that connect the two atomic layers of Mn. As a result, this system exhibits  $f$ -wave altermagnetism, with the pronounced symmetrical spin splitting occurring predominantly in the Mn  $3d$  orbital-contributed bands (see Fig. S4), following the electron occupancy index of No. 83 (corresponding to the zero-order band component).

As summarized in Table I, the stacking sliding of the second layer results in two additional symmetries, represented by space groups No. 12 ( $C2/m$ ) and No. 2 ( $P\bar{1}$ ). For the first case, we consider  $\{E|\frac{1}{2}, 0\}$  as a representative example (designated as sliding B), in which only the symmetries  $[C_2||P]$  and  $[E||C_{2y}T]$  survive. This configuration protects the spin-degenerate line at  $k_{a^*} = 0$ , as depicted in Fig. 3(d). Therefore, the  $f$ -wave altermagnet degrades to the  $p$ -wave one. Despite this degradation, the opposite spin splitting remains evident along the corresponding reciprocal lines [see Figs. 3(c) and 3(d)], continuing to support the presence of odd-parity altermagnetism. Furthermore, the space group No. 2 ( $P\bar{1}$ ) retains merely  $[C_2||P]$ , which links the two Mn atoms with opposite magnetic moments. This symmetrical operator enforces the relation  $\varepsilon(\mathbf{k}, s) = \varepsilon(-\mathbf{k}, -s)$ , thereby necessitating spin degeneracy at the  $\Gamma$  point ( $k_{a^*} = k_{b^*} = 0$ ). This configuration also represents an odd-parity,  $p$ -wave altermagnet, as illustrated in Figs. 3(e) and 3(f), with  $\{E|\frac{1}{3}, 0\}$  serving as a representative example (designated as sliding C). In this case, all spin-degenerate lines (depicted in white) are absent, while the energy of spin splitting is distributed around the  $\Gamma$  point in an antisymmetric manner.

Markedly, when the direction of the incident CPL deviates from the  $z$ -axis, the  $C_{3z}$ -rotational symmetry is broken, leading to the loss of  $f$ -wave characteristics. However, the  $p$ -wave altermagnetic states remain intact. For stacking configurations A to C, we have compiled the remaining symmetry operations in Tables S1 to S3 in the supplementary materials, categorized according to four conditions: incident direction along the  $z$ -axis,  $x$ -axis,  $y$ -axis, and other orientations. Additionally, for stacking sliding A of BL-MBT, Fig. S3 reveals the spin-resolved band structures and the distributions of spin-splitting energies across the entire BZ for the three incident angles: along  $x$ -axis,  $y$ -axis, and other direction. These results confirm the theoretical analysis of spin-space symmetries,

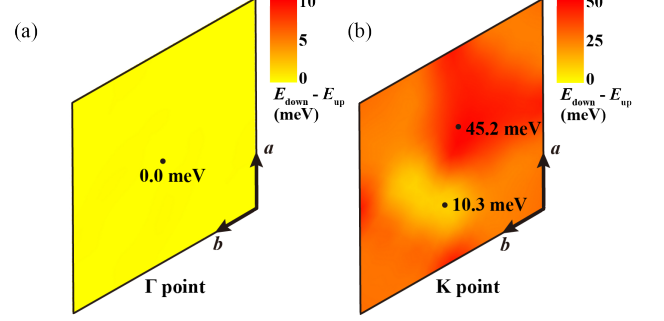


FIG. 4. **The stacking-sliding invariance of Floquet-altermagnets in BL-MBT.** Subfigures (a) and (b) demonstrate the spin-splitting energies at the  $\Gamma$  and  $K$  points distributing across the entire sliding zone, respectively. The color gradient, ranging from yellow to red, represents the relationship:  $E_{\text{down}} - E_{\text{up}}$ , with the light incident direction oriented along the  $z$  axis.

with  $[C_2||P]$  consistently surviving. Furthermore, a detailed examination of the theoretical analysis on forward stacking of BL-MBT is presented in Sec. I of the supplementary materials.

In addition to the previously discussed three representatives, we now underscore the stacking-sliding invariance of odd-parity altermagnetic states. Figure 4 illustrates this novel feature, showcasing the spin-splitting distributions across the entire stacking-sliding zone at the  $\Gamma$  [Fig. 4(a)] and  $K$  [Fig. 4(b)] points, respectively. In like manner, the light frequency and intensity are fixed at  $\hbar\omega = 9.0 \text{ eV}$  and  $0.3 \text{ \AA}^{-1}$ , with the band index (electron occupancy) set to No. 83. Absolutely, no spin splitting is observed at the  $\Gamma$  point, while the spin splitting at the  $K$  point permeates the entire stacking-sliding zone, the values ranging from 10.3 meV to 45.2 meV. This observation rigorously confirms the stacking-sliding invariance of Floquet-induced altermagnetism in forward-stacking BL-MBT.

Unfortunately, when BL-MBT is stacked in reverse, as displayed in the side view of Fig. S5(a), the symmetry  $[C_2||P]$  is lost and replaced by  $[C_2||M_z]$ . This alteration results in a transition to space group No. 187 ( $P\bar{6}m2$ ), which preserves  $C_{3z}$ -rotational symmetry but loses inversion symmetry. The  $[C_2||M_z]$  configuration leads to spin degeneracy throughout the entire BZ, resulting in an AFM state. However, when light is incident along the  $x$ -axis, the  $[C_2||M_z]$  symmetry is broken, enabling the emergence of a  $p$ -wave altermagnetic state. At arbitrary angles of CPL, there are no spin-space symmetric operators that connect the two Mn atoms with opposite spins, resulting in a compensated ferrimagnetic (CFiM) state [75] characterized by spin-splitting throughout the entire BZ. Thus, in the absence of the protection afforded by  $[C_2||P]$ , the altermagnetic state loses its invariance with

respect to the CPL incident angle. Detailed results pertaining to space group No. 187 for the reversed stacking configuration can be found in Table S4 and Fig. S5 in Secs. I and IV of the supplementary materials.

Additionally, the reversed stacking-sliding configuration gives rise to five additional space groups: No. 156 ( $P3m1$ ), No. 39 ( $Aem2$ ), No. 8 ( $Cm$ ), No. 5 ( $C2$ ) and No. 1 ( $P1$ ). Among these, only space groups No. 39 ( $Aem2$ ) and No. 5 ( $C2$ ) permit the emergence of  $p$ -wave altermagnetism, contingent upon specific incident directions. In contrast, the CFiM state remains stable under all conditions for the other three space groups. Detailed analyses can be found in Tables S5-S10 in Sec. I of the supplementary materials.

In summary, we investigate and characterize the invariance of Floquet altermagnetism in A-AFM bilayers concerning stacking sliding and light illumination direction, assuming the presence of inversion symmetry. Symmetrical analysis with spin-space groups, in conjunction with light illumination, supports this conclusion. We propose a straightforward strategy to construct A-AFM bilayers with inversion symmetry from any arbitrary FM monolayers, guided by the  $d$ -electron counting rule. Then, using forward-stacking BL-MBT as a representative template, we demonstrate the existence of an  $f$ -wave altermagnet under stacking-sliding arrangements within space

group No. 164, illuminated by out-of-plane CPL. In contrast, a  $p$ -wave state emerges under alternative conditions. Even if the in-plane mirror symmetry exists, the altermagnetism remains invariant by only excluding out-of-plane irradiation. Our findings and proposals significantly popularize the material design of altermagnets; specifically, if an AFM-coupled bilayer is constructed from two FM monolayers with inversion symmetry, it must be a CPL- or EPL-induced altermagnet.

## ACKNOWLEDGMENTS

We thank Prof. Huisheng Zhang, Dr. Xiyu Hong, Dr. Chaoxi Cui, Ling Bai, Jingjing Cao and Wenlu Zhang for helpful discussions, and thank Asso. Prof. Huixia Fu, Dr. Hang Liu for technical supports. The numerical calculations have been done on the supercomputing system in the Huairou Materials Genome Platform. This work is supported by National Natural Science Foundation of China (Grant Nos. 12025407, 12450401, 12104072 and 12304536), National Key Research and Development Program of China (Grant No. 2021YFA1400201), and Chinese Academy of Sciences (Grant Nos. YSBR-047 and No. XDB33030100).

Zhe Li and Lijuan Li contributed equally to this work.

- 
- [1] L. Šmejkal, J. Sinova, and T. Jungwirth, Beyond conventional ferromagnetism and antiferromagnetism: A phase with nonrelativistic spin and crystal rotation symmetry, *Physical Review X* **12**, 031042 (2022).
- [2] L. Šmejkal, J. Sinova, and T. Jungwirth, Emerging research landscape of altermagnetism, *Physical Review X* **12**, 040501 (2022).
- [3] L. Bai, W. Feng, S. Liu, L. Šmejkal, Y. Mokrousov, and Y. Yao, Altermagnetism: Exploring new frontiers in magnetism and spintronics, *Advanced Functional Materials* **34**, 2409327 (2024).
- [4] C. Song, H. Bai, Z. Zhou, L. Han, H. Reichlova, J. H. Dil, J. Liu, X. Chen, and F. Pan, Altermagnets as a new class of functional materials, *Nature Reviews Materials* **10**, 473 (2025).
- [5] W. Xun, X. Liu, Y. Zhang, Y.-Z. Wu, and P. Li, Stacking-, strain-engineering induced altermagnetism, multipiezo effect, and topological state in two-dimensional materials, *Applied Physics Letters* **126**, 161903 (2025).
- [6] Y. Zhu, M. Gu, Y. Liu, X. Chen, Y. Li, S. Du, and Q. Liu, Sliding ferroelectric control of unconventional magnetism in stacked bilayers, *Physical Review Letters* **135**, 056801 (2025).
- [7] X. Chen, J. Ren, Y. Zhu, Y. Yu, A. Zhang, P. Liu, J. Li, Y. Liu, C. Li, and Q. Liu, Enumeration and representation theory of spin space groups, *Physical Review X* **14**, 031038 (2024).
- [8] X. Chen, Y. Liu, P. Liu, Y. Yu, J. Ren, J. Li, A. Zhang, and Q. Liu, Unconventional magnons in collinear magnets dictated by spin space groups, *Nature* **640**, 349 (2025).
- [9] M. Gu, Y. Liu, H. Zhu, K. Yananose, X. Chen, Y. Hu, A. Stroppa, and Q. Liu, Ferroelectric switchable altermagnetism, *Physical Review Letters* **134**, 106802 (2025).
- [10] X. Duan, J. Zhang, Z. Zhu, Y. Liu, Z. Zhang, I. Žutić, and T. Zhou, Antiferroelectric altermagnets: Antiferroelectricity alters magnets, *Physical Review Letters* **134**, 106801 (2025).
- [11] J. Krempaský, L. Šmejkal, S. D'souza, M. Hajlaoui, G. Springholz, K. Uhlířová, F. Alarab, P. Constantinou, V. Strocov, D. Usanov, *et al.*, Altermagnetic lifting of Kramers spin degeneracy, *Nature* **626**, 517 (2024).
- [12] S. Lee, S. Lee, S. Jung, J. Jung, D. Kim, Y. Lee, B. Seok, J. Kim, B. G. Park, L. Šmejkal, *et al.*, Broken Kramers degeneracy in altermagnetic MnTe, *Physical Review Letters* **132**, 036702 (2024).
- [13] Z. Liu, M. Ozeki, S. Asai, S. Itoh, and T. Masuda, Chiral split magnon in altermagnetic MnTe, *Physical Review Letters* **133**, 156702 (2024).
- [14] J. Ding, Z. Jiang, X. Chen, Z. Tao, Z. Liu, T. Li, J. Liu, J. Sun, J. Cheng, J. Liu, *et al.*, Large band splitting in  $g$ -wave altermagnet CrSb, *Physical Review Letters* **133**, 206401 (2024).
- [15] M. Zeng, M.-Y. Zhu, Y.-P. Zhu, X.-R. Liu, X.-M. Ma, Y.-J. Hao, P. Liu, G. Qu, Y. Yang, Z. Jiang, *et al.*, Observation of spin splitting in room-temperature metallic antiferromagnet CrSb, *Advanced Science* **11**, 2406529 (2024).
- [16] G. Yang, Z. Li, S. Yang, J. Li, H. Zheng, W. Zhu, Z. Pan, Y. Xu, S. Cao, W. Zhao, *et al.*, Three-dimensional mapping of the altermagnetic spin splitting in CrSb, *Nature Communications* **16**, 1442 (2025).

- [17] L. Šmejkal, A. Marmodoro, K.-H. Ahn, R. González-Hernández, I. Turek, S. Mankovsky, H. Ebert, S. W. D'Souza, O. Šipr, J. Sinova, *et al.*, Chiral magnons in altermagnetic RuO<sub>2</sub>, *Physical Review Letters* **131**, 256703 (2023).
- [18] Z. Feng, X. Zhou, L. Šmejkal, L. Wu, Z. Zhu, H. Guo, R. González-Hernández, X. Wang, H. Yan, P. Qin, *et al.*, An anomalous Hall effect in altermagnetic ruthenium dioxide, *Nature Electronics* **5**, 735 (2022).
- [19] H. Bai, L. Han, X. Feng, Y. Zhou, R. Su, Q. Wang, L. Liao, W. Zhu, X. Chen, F. Pan, *et al.*, Observation of spin splitting torque in a collinear antiferromagnet RuO<sub>2</sub>, *Physical Review Letters* **128**, 197202 (2022).
- [20] X. Zhou, W. Feng, R.-W. Zhang, L. Šmejkal, J. Sinova, Y. Mokrousov, and Y. Yao, Crystal thermal transport in altermagnetic RuO<sub>2</sub>, *Physical Review Letters* **132**, 056701 (2024).
- [21] B. Jiang, M. Hu, J. Bai, Z. Song, C. Mu, G. Qu, W. Li, W. Zhu, H. Pi, Z. Wei, *et al.*, A metallic room-temperature *d*-wave altermagnet, *Nature Physics* **21**, 754 (2025).
- [22] Y. Xu, H. Zhang, M. Feng, and F. Tian, Electronic structure, magnetic transition, and fermi surface instability of the room-temperature altermagnet KV<sub>2</sub>Se<sub>2</sub>O, *Physical Review B* **112**, 125141 (2025).
- [23] F. Zhang, X. Cheng, Z. Yin, C. Liu, L. Deng, Y. Qiao, Z. Shi, S. Zhang, J. Lin, Z. Liu, *et al.*, Crystal-symmetry-paired spin-valley locking in a layered room-temperature antiferromagnet, *arXiv preprint arXiv:2407.19555* (2024).
- [24] W. Xie, X. Xu, Y. Yue, H. Xia, and H. Wang, Piezovally effect and magnetovally coupling in altermagnetic semiconductors studied by first-principles calculations, *Physical Review B* **111**, 134429 (2025).
- [25] P. Feng, C.-Y. Tan, M. Gao, X.-W. Yan, Z.-X. Liu, P.-J. Guo, F. Ma, and Z.-Y. Lu, Type-II quantum spin Hall insulator, *arXiv preprint arXiv:2503.13397* (2025).
- [26] X. Zou, X. Feng, Y. Dai, B. Huang, and C. Niu, Floquet quantum anomalous Hall effect with in-plane magnetization in two-dimensional altermagnets, *ACS Nano* **19**, 35575 (2025).
- [27] B. Pan, P. Zhou, P. Lyu, H. Xiao, X. Yang, and L. Sun, General stacking theory for altermagnetism in bilayer systems, *Physical Review Letters* **133**, 166701 (2024).
- [28] S. Zeng and Y.-J. Zhao, Bilayer stacking A-type altermagnet: A general approach to generating two-dimensional altermagnetism, *Physical Review B* **110**, 174410 (2024).
- [29] Y. Zhu, T. Chen, Y. Li, L. Qiao, X. Ma, C. Liu, T. Hu, H. Gao, and W. Ren, Multipiezo effect in altermagnetic V<sub>2</sub>SeTeO monolayer, *Nano Letters* **24**, 472 (2023).
- [30] I. I. Mazin, K. Koepernik, M. D. Johannes, R. González-Hernández, and L. Šmejkal, Prediction of unconventional magnetism in doped FeSb<sub>2</sub>, *Proceedings of the National Academy of Sciences* **118**, e2108924118 (2021).
- [31] S. Bhowal and N. A. Spaldin, Ferroically ordered magnetic octupoles in *d*-wave altermagnets, *Physical Review X* **14**, 011019 (2024).
- [32] V. C. Morano, Z. Maesen, S. E. Nikitin, J. Lass, D. G. Mazzone, and O. Zaharko, Absence of altermagnetic magnon band splitting in MnF<sub>2</sub>, *Physical Review Letters* **134**, 226702 (2025).
- [33] Y. Guo, H. Liu, O. Janson, I. C. Fulga, J. van den Brink, and J. I. Facio, Spin-split collinear antiferromagnets: A large-scale ab-initio study, *Materials Today Physics* **32**, 100991 (2023).
- [34] M. Leiviskä, J. Rial, A. Bad'ura, R. L. Seeger, I. Kounta, S. Beckert, D. Kriegner, I. Joumard, E. Schmoranzzerová, J. Sinova, *et al.*, Anisotropy of the anomalous Hall effect in thin films of the altermagnet candidate Mn<sub>5</sub>Si<sub>3</sub>, *Physical Review B* **109**, 224430 (2024).
- [35] H. Reichlova, R. Lopes Seeger, R. González-Hernández, I. Kounta, R. Schlitz, D. Kriegner, P. Ritzinger, M. Lamme, M. Leiviskä, A. Birk Hellenes, *et al.*, Observation of a spontaneous anomalous Hall response in the Mn<sub>5</sub>Si<sub>3</sub> *d*-wave altermagnet candidate, *Nature Communications* **15**, 4961 (2024).
- [36] A. Badura, W. H. Campos, V. K. Bharadwaj, I. Kounta, L. Michez, M. Petit, J. Rial, M. Leiviskä, V. Baltz, F. Krizek, *et al.*, Observation of the anomalous Nernst effect in altermagnetic candidate Mn<sub>5</sub>Si<sub>3</sub>, *Nature Communications* **16**, 7111 (2025).
- [37] N. Wang, J. Chen, N. Ding, H. Zhang, S. Dong, and S.-S. Wang, Magneto-optical Kerr effect and magnetoelasticity in weak ferromagnetic RuF<sub>4</sub> monolayer, *arXiv preprint arXiv:2209.00178* (2022).
- [38] T. Sato, S. Haddad, I. C. Fulga, F. F. Assaad, and J. van den Brink, Altermagnetic anomalous Hall effect emerging from electronic correlations, *Physical Review Letters* **133**, 086503 (2024).
- [39] H.-Z. Liu, R. He, J.-Y. Zhan, D. Wang, M.-D. He, N. Luo, J. Zeng, K.-Q. Chen, and L.-M. Tang, Anomalous Hall effect in A-type antiferromagnetic bilayers, *Physical Review B* **112**, 134411 (2025).
- [40] X.-J. Yi, Y. Mao, X. Lu, and Q.-F. Sun, Spin splitting Nernst effect in altermagnets, *Physical Review B* **111**, 035423 (2025).
- [41] Y. Jiang, X. Zhang, H. Bai, Y. Tian, B. Zhang, W.-J. Gong, and X. Kong, Strain-engineering spin-valley locking effect in altermagnetic monolayer with multipiezo properties, *Applied Physics Letters* **126**, 053102 (2025).
- [42] M. N. Blonsky, H. L. Zhuang, A. K. Singh, and R. G. Hennig, Ab initio prediction of piezoelectricity in two-dimensional materials, *ACS Nano* **9**, 9885 (2015).
- [43] R. González-Hernández, L. Šmejkal, K. Vyboryň, Y. Yahagi, J. Sinova, T. Jungwirth, and J. Železný, Efficient electrical spin splitter based on nonrelativistic collinear antiferromagnetism, *Physical Review Letters* **126**, 127701 (2021).
- [44] X. Zhou, W. Feng, X. Yang, G.-Y. Guo, and Y. Yao, Crystal chirality magneto-optical effects in collinear antiferromagnets, *Physical Review B* **104**, 024401 (2021).
- [45] W. Sun, H. Ye, L. Liang, N. Ding, S. Dong, and S.-S. Wang, Stacking-dependent ferroicity of a reversed bilayer: Altermagnetism or ferroelectricity, *Physical Review B* **110**, 224418 (2024).
- [46] Z. Zhang, Y. Bai, X. Zou, B. Huang, Y. Dai, and C. Niu, Altermagnetic quantum spin Hall effect in a Chern homobilayer, *Physical Review B* **112**, 085128 (2025).
- [47] S. Huang, Z. Qin, F. Zhan, D.-H. Xu, D.-S. Ma, and R. Wang, Light-induced odd-parity magnetism in conventional collinear antiferromagnets, *arXiv preprint arXiv:2507.20705* (2025).
- [48] B. Li, D.-F. Shao, and A. A. Kovalev, Floquet spin splitting and spin generation in antiferromagnets, *arXiv preprint arXiv:2507.22884* (2025).
- [49] T. Zhu, D. Zhou, H. Wang, and J. Ruan, Floquet odd-parity collinear magnets, *arXiv preprint*

- arXiv:2508.02542 (2025).
- [50] D. Liu, Z.-Y. Zhuang, D. Zhu, Z. Wu, and Z. Yan, Light-induced odd-parity altermagnets on dimerized lattices, arXiv preprint arXiv:2508.18360 (2025).
- [51] X.-J. Luo, J.-X. Hu, and K. Law, Spin symmetry criteria for odd-parity magnets, arXiv preprint arXiv:2510.05512 (2025).
- [52] J. Xiao and B. Yan, An electron-counting rule to determine the interlayer magnetic coupling of the van der Waals materials, *2D Materials* **7**, 045010 (2020).
- [53] Z. Li, J. Li, K. He, X. Wan, W. Duan, and Y. Xu, Tunable interlayer magnetism and band topology in van der waals heterostructures of  $\text{MnBi}_2\text{Te}_4$ -family materials, *Physical Review B* **102**, 081107 (2020).
- [54] X.-Y. Tang, Z. Li, F. Xue, P. Ji, Z. Zhang, X. Feng, Y. Xu, Q. Wu, and K. He, Intrinsic and tunable quantum anomalous Hall effect and magnetic topological phases in  $\text{XYBi}_2\text{Te}_5$ , *Physical Review B* **108**, 075117 (2023).
- [55] G. Qiu, Q. Nian, M. Motlag, S. Jin, B. Deng, Y. Deng, A. R. Charnas, P. D. Ye, and G. J. Cheng, Ultrafast laser-shock-induced confined metaphase transformation for direct writing of black phosphorus thin films, *Advanced Materials* **30**, 1704405 (2018).
- [56] Z. Li, H. Cao, and S. Meng, Light-induced above-room-temperature Chern insulators in group-IV Xenes, *npj Computational Materials* **11**, 160 (2025).
- [57] Z. Li, H. Cao, and S. Meng, Laser-engineered  $\gamma$ -point topology in trigonal bismuthene, arXiv preprint arXiv:2509.08068 (2025).
- [58] Z. Li, F. Zhan, H. Cao, J. Cao, H. Zhang, and S. Meng, Light-engineered multichannel quantum anomalous Hall effect in high-order topological plumbene, arXiv preprint arXiv:2511.18520 (2025).
- [59] H. Liu, H. Cao, and S. Meng, Floquet engineering of topological states in realistic quantum materials via light-matter interactions, *Progress in Surface Science* **98**, 100705 (2023).
- [60] M. Bukov, L. D'Alessio, and A. Polkovnikov, Universal high-frequency behavior of periodically driven systems: from dynamical stabilization to Floquet engineering, *Advances in Physics* **64**, 139 (2015).
- [61] S. Blanes, F. Casas, J.-A. Oteo, and J. Ros, The Magnus expansion and some of its applications, *Physics Reports* **470**, 151 (2009).
- [62] J. Li, Y. Li, S. Du, Z. Wang, B.-L. Gu, S.-C. Zhang, K. He, W. Duan, and Y. Xu, Intrinsic magnetic topological insulators in van der waals layered  $\text{MnBi}_2\text{Te}_4$ -family materials, *Science Advances* **5**, eaaw5685 (2019).
- [63] Y. Li, J. Li, Y. Li, M. Ye, F. Zheng, Z. Zhang, J. Fu, W. Duan, and Y. Xu, High-temperature quantum anomalous Hall insulators in lithium-decorated iron-based superconductor materials, *Physical Review Letters* **125**, 086401 (2020).
- [64] M. M. Otrokov, I. I. Klimovskikh, H. Bentmann, D. Eshyuni, A. Zeugner, Z. S. Aliev, S. Gaß, A. Wolter, A. Koroleva, A. M. Shikin, *et al.*, Prediction and observation of an antiferromagnetic topological insulator, *Nature* **576**, 416 (2019).
- [65] M. Otrokov, I. P. Rusinov, M. Blanco-Rey, M. Hoffmann, A. Y. Vyazovskaya, S. V. Eremeev, A. Ernst, P. M. Echenique, A. Arnau, and E. V. Chulkov, Unique thickness-dependent properties of the van der waals interlayer antiferromagnet  $\text{MnBi}_2\text{Te}_4$  films, *Physical Review Letters* **122**, 107202 (2019).
- [66] D. Zhang, M. Shi, T. Zhu, D. Xing, H. Zhang, and J. Wang, Topological axion states in the magnetic insulator  $\text{MnBi}_2\text{Te}_4$  with the quantized magnetoelectric effect, *Physical Review Letters* **122**, 206401 (2019).
- [67] J. Zhang, D. Wang, M. Shi, T. Zhu, H. Zhang, and J. Wang, Large dynamical axion field in topological antiferromagnetic insulator  $\text{Mn}_2\text{Bi}_2\text{Te}_5$ , *Chinese Physics Letters* **37**, 077304 (2020).
- [68] Y. Deng, Y. Yu, M. Z. Shi, Z. Guo, Z. Xu, J. Wang, X. H. Chen, and Y. Zhang, Quantum anomalous hall effect in intrinsic magnetic topological insulator  $\text{MnBi}_2\text{Te}_4$ , *Science* **367**, 895 (2020).
- [69] Y. Gong, J. Guo, J. Li, K. Zhu, M. Liao, X. Liu, Q. Zhang, L. Gu, L. Tang, X. Feng, *et al.*, Experimental realization of an intrinsic magnetic topological insulator, *Chinese Physics Letters* **36**, 076801 (2019).
- [70] C. Liu, Y. Wang, H. Li, Y. Wu, Y. Li, J. Li, K. He, Y. Xu, J. Zhang, and Y. Wang, Robust axion insulator and chern insulator phases in a two-dimensional antiferromagnetic topological insulator, *Nature Materials* **19**, 522 (2020).
- [71] J. Ge, Y. Liu, J. Li, H. Li, T. Luo, Y. Wu, Y. Xu, and J. Wang, High-Chern-number and high-temperature quantum Hall effect without Landau levels, *National Science Review* **7**, 1280 (2020).
- [72] Y. Bai, Y. Li, J. Luan, R. Liu, W. Song, Y. Chen, P.-F. Ji, Q. Zhang, F. Meng, B. Tong, *et al.*, Quantized anomalous Hall resistivity achieved in molecular beam epitaxy-grown  $\text{MnBi}_2\text{Te}_4$  thin films, *National Science Review* **11**, nwad189 (2024).
- [73] Z. Li, J. Zhang, X. Hong, X. Feng, and K. He, Multi-mechanism quantum anomalous Hall and Chern number tunable states in germanene (silicene, stanene)/ $\text{MBi}_2\text{Te}_4$  heterostructures, *Physical Review B* **109**, 235132 (2024).
- [74] Z. Li, F. Xue, X.-Y. Tang, X. Hong, Y. Chen, X. Feng, and K. He, Universally optimizable strategy for magnetic gaps towards high-temperature quantum anomalous Hall states via magnetic-insulator/topological-insulator building blocks, *Physical Review B* **111**, 075106 (2025).
- [75] Y. Liu, Y. Liu, X. Wang, N. Xia, G. Xu, Y. Wang, H. Wang, W. Gao, and J. Zhao, Robust altermagnetism and compensated ferrimagnetism in  $\text{MnP}X_3$ -based ( $X=\text{S}$  or  $\text{Se}$ ) heterostructures, *Physical Review Materials* **9**, 104406 (2025).